

Phase competition and anomalous thermal evolution in high-temperature superconductorsZuo-Dong Yu,¹ Yuan Zhou,^{1,2,3,*} Wei-Guo Yin,^{2,†} Hai-Qing Lin,⁴ and Chang-De Gong^{5,1,3}¹*National Laboratory of Solid State Microstructure, Department of Physics, Nanjing University, Nanjing 210093, China*²*Condensed Matter Physics and Materials Science Department, Brookhaven National Laboratory, Upton, New York 11973, USA*³*Collaborative Innovation Center of Advanced Microstructures, Nanjing University, Nanjing 210093, China*⁴*Beijing Computational Science Research Center, Beijing 100084, China*⁵*Center for Statistical and Theoretical Condensed Matter Physics, Zhejiang Normal University, Jinhua 321004, China*

(Received 11 November 2016; revised manuscript received 22 June 2017; published 12 July 2017)

The interplay of competing orders is relevant to high-temperature superconductivity known to emerge upon suppression of a parent antiferromagnetic order typically via charge doping. How such interplay evolves at low temperature—in particular at what doping level the zero-temperature quantum critical point (QCP) is located—is still elusive because it is masked by the superconducting state. The QCP had long been believed to follow a smooth extrapolation of the characteristic temperature T^* for the strange normal state well above the superconducting transition temperature. However, recently the T^* within the superconducting dome was reported to unexpectedly exhibit back-bending likely in the cuprate $\text{Bi}_2\text{Sr}_2\text{CaCu}_2\text{O}_{8+\delta}$. Here we show that the original and revised phase diagrams can be understood in terms of weak and moderate competitions, respectively, between superconductivity and a pseudogap state such as d -density or spin-density wave, based on both Ginzburg-Landau theory and the realistic t - t' - t'' - J - V model for the cuprates. We further found that the calculated temperature and doping-level dependence of the quasiparticle spectral gap and Raman response qualitatively agrees with the experiments. In particular, the T^* back-bending can provide a simple explanation of the observed anomalous two-step thermal evolution dominated by the superconducting gap and the pseudogap, respectively. Our results imply that the revised phase diagram is likely to take place in high-temperature superconductors.

DOI: [10.1103/PhysRevB.96.045110](https://doi.org/10.1103/PhysRevB.96.045110)**I. INTRODUCTION**

The rich phase diagrams of correlated electron materials are a central concern in both condensed matter physics and technological applications [1–3]. One archetypical example is the emergence of superconductivity (SC) upon suppression of a “parent” electronic order typically by doping. This generally yields a dome structure of the SC critical temperature T_c as a function of the doping level x . The parent competing order (CO) ranges from the antiferromagnetic spin order in cuprates [4–8] and heavy-fermion rare-earth compounds [9], to the ferro-orbital and antiferromagnetic spin dipolar/quadrupolar orders in iron pnictides/chalcogenides [10–13], and to the charge order in titanium oxypnictides [14] and transition-metal dichalcogenides [15]. A particularly interesting case is the cuprate high-temperature superconductors, where the parent and SC phases do not appear to coexist but the phase competition is actually intensified by the emergence of a “strange metal” normal state with pseudogap opening at a temperature T^* well above T_c in the underdoped regime [5]. The origin of the pseudogap has been controversial, being attributed to the pre-formation of Cooper pairs [16–21] or a hidden CO such as a d -density wave (DDW) [22–27], spin-density wave (SDW) [28–31], loop-current [32], nematic or stripe order [33–38], pair density wave [39,40], etc. It has been observed that upon doping, T^* decreases gradually in the normal state above the T_c dome, and enters into the SC dome near the optimal doping level at x_{OP} . To date, how T^* evolves with doping under the T_c dome is a key missing piece of the pseudogap puzzle [6,7]. The conventional notion [4,5]

is that T^* follows smoothly its normal-state behavior and ends ($T^* = 0$) at the quantum critical point (QCP) $x_{\text{QCP}} > x_{\text{OP}}$ in the overdoped regime [see Fig. 1(a)].

However, a revised phase diagram was suggested by some recent angle-resolved photoemission spectroscopy (ARPES) measurements in $\text{Bi}_2\text{Sr}_2\text{CaCu}_2\text{O}_{8+\delta}$ (Bi-2212) cuprates [41,42]: at slight overdoping, the system seems to change from a coexisting pseudogap-SC state to the pure SC state as temperature decreases to zero, leading to a back-bending behavior of T^* as a function of x under the T_c dome [cf. Fig. 1(b)]. This possibility stimulates new thinking about the phase competition in the high- T_c superconductors. For example, can the existence or nonexistence of the T^* back-bending be able to confirm or rule out some proposed COs as the pseudogap state? Interestingly, a similar back-bending phenomenon and revised phase diagram was clearly established in the iron-based high- T_c superconductor $\text{Ba}(\text{Fe}_{1-x}\text{Co}_x)_2\text{As}_2$ (Ba-122) [43–45], where the QCP is located at the underdoped region, i.e., $x_{\text{QCP}} < x_{\text{OP}}$ [see Figs. 1(c) and 1(d)], although undoped iron pnictides are bad metals rather than Mott insulators like cuprates.

Theoretically, a back bending of T^* was obtained in a simple Landau theory for certain competition between two orders [46]. Thus the revised phase diagram can happen, in principle, but whether it does take place in real materials or the realistic microscopic models for them remains elusive. A mean-field-type theory of the t - J model for the cuprates [26,27] predicted a “pre-back-bending” of T^* due to DDW, namely it starts well above the T_c dome and even exists without SC, in disagreement with what was suggested above by the Landau theory and the ARPES data.

The ultimate detection and comprehensive understanding of the revised phase diagram demand a study of how it is related to the many unusual spectroscopy observations.

*zhouyuan@nju.edu.cn

†wyin@bnl.gov

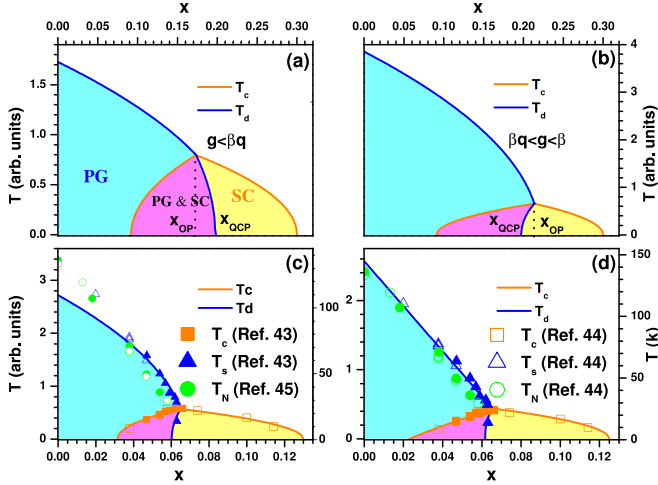


FIG. 1. Phase diagrams of the competing SC (yellow), CO (cyan), and coexisting (pink) states in Ginzburg-Landau theory. (a) The original type, where $x_{QCP} > x_{OP}$, for $g = 1$. (b) The revised type, where $x_{QCP} < x_{OP}$, for $g = 0.2$. The other parameters are $\alpha_s(x) = 10(x - 0.3)$, $\alpha_d(x) = 27(x - 0.22)$, $\beta = 2$, and $g = 1.2$ used in Ref. [46] for cuprates. Lower panels are our fits to the experimental data (various symbols) on Ba-122 iron-pnictides [43–45] using (c) Eq. (3) with $\alpha_s(x) = 10(x - 0.13)$, $\alpha_d(x) = 50(x - 0.068)$, $q = 0.23$, $\beta = 2$, $g = 1.1$, and (d) Eq. (4) with $\alpha_s(x) = 10(x - 0.125)$, $\alpha_d(x) = 26(x - 0.079)$, $q = 0.4$, $p = 0.3$, $\beta = 2$, $g = 1.4$.

For example, previous ARPES measurements showed clear evidence that the antinodal gap is enhanced with temperature at optimally doped $\text{Bi}_2\text{Sr}_2\text{CuO}_{6+\delta}$ (Bi-2201) [47,48] and $\text{La}_{2-x}\text{Sr}_x\text{CuO}_4$ (La-214) [49]. A recent study on Bi-2201 further reported that the anomalous temperature dependence of the measured gap, from slight underdoping to slight overdoping, extends to temperatures above T_c (below T^*) [50]. In comparison, the gap remains nearly unchanged below T_c in the deeply underdoped region where the pseudogap dominates, but follows the traditional BCS-like temperature dependence in the heavily overdoped region where the SC gap dominates. Moreover, the gap evolution can be clearly detected by electronic Raman scattering (ERS) as well. By choosing the incident and scattered light polarization vectors, one can probe the gap magnitude in different regions of the Brillouin zone (BZ). In particular, the B_{1g} and B_{2g} channels measure the gap features of the antinodal and nodal regions, respectively [51]. The antinodal and nodal gaps, considered to be pseudogap and SC dominated, respectively, exhibit distinct doping dependence [52–58]. Their temperature evolution in slightly underdoped cuprates is rather unexpected; the gap extracted from the B_{1g} channel remains nearly unchanged or even increases as temperature increases toward T_c , rather than decreasing to zero as predicted by the standard BCS theory for d -wave SC. Similar enhancement in the ERS signals was discovered in lightly underdoped iron-pnictide Ba-122 [59], further indicating a close connection between the cuprate and iron-pnictide high- T_c superconductors.

Here, we carry out a systematical study of the phase competition between SC and a CO using both Ginzburg-Landau theory (Sec. II) and different mean-field theories of the extended t - J model for the cuprates (Sec. III). We

show that the revised and original phase diagrams in high- T_c superconductors can be established with the moderate and weak competitions, respectively. In the latter microscopic model, the nearest-neighbor Coulomb interaction V as well as the second and third nearest-neighbor hopping integrals t' and t'' are included to tune the competition. We found that the back-bending of T^* under the T_c dome is quite robust against those parameter tunings but t' is necessary to prevent the pre-back-bending of T^* in the absence of SC. Inclusion of the much neglected feedback effect of SC on pseudogap can push the back-bending point from optimal doping to the overdoped regime, in better agreement with the experiments [41,42]. In Sec. IV, we calculate out the ARPES and ERS spectral functions in mean-field theory of the realistic t - t' - t'' - J - V model to reveal that the back-bending of T^* can provide a simple explanation of the observed anomalous temperature dependence of the antinodal gap via a two-step evolution where the SC and CO dominate low- and high-temperature regions, respectively. In Sec. V, we consider SDW and show that it produces a less severe back-bending of T^* and worse agreement with ERS than DDW. The implications of our results are discussed in Sec. VI and the paper is summarized in Sec. VII.

II. GINZBURG-LANDAU THEORY

To evaluate the competition between SC and a CO, we start with the standard free energy [46,60]:

$$F = \alpha_s(x, T)|\psi|^2 + \frac{\beta_s}{2}|\psi|^4 + \alpha_d(x, T)\phi^2 + \frac{\beta_d}{2}\phi^4 + g|\psi|^2\phi^2, \quad (1)$$

where ψ and ϕ are the order parameter for SC and the CO, respectively; g is the interaction constant between them. Here we use the critical temperature T_d for the CO to approximate T^* for the pseudogap.

For simplicity, we set $\beta_s = \beta_d = \beta$ and assume that $\alpha_{s,d}(x, T)$ are the only parameters that bear the x and T dependence, taking the form

$$\alpha_{s,d}(x, T) = \alpha_{s,d}(x) + \gamma_{s,d}^{(1)}T + \gamma_{s,d}^{(2)}T^2. \quad (2)$$

In particular, the pure quadratic T dependence introduced by Wu *et al.* [46] to reproduce the desired form of $\alpha_s(x, T) \simeq 2\beta T_c(T - T_c)$ near T_c reads

$$\begin{aligned} \alpha_s(x, T) &= \alpha_s(x) + \beta T^2, \\ \alpha_d(x, T) &= \alpha_d(x) + q\beta T^2. \end{aligned} \quad (3)$$

When the two orders are decoupled, $T_c = \sqrt{-\alpha_s(x)/\beta}$ and $T_d = \sqrt{-\alpha_d(x)/q\beta}$. Here the q factor describes the CO's relative tolerance to thermal suppression: the smaller q , the more tolerant the CO than SC [46]. It is shown that decreasing q can change the phase diagram from the original type realized for $q > g/\beta$ [Fig. 1(a)] to the revised type realized for $q < g/\beta < 1$ [Fig. 1(b)].

The phase diagram also depends sensitively on g , the interaction strength, as it is equally fair to read that increasing g can change the phase diagram from the original type realized for $g < q\beta$ [Fig. 1(a)] to the revised type realized

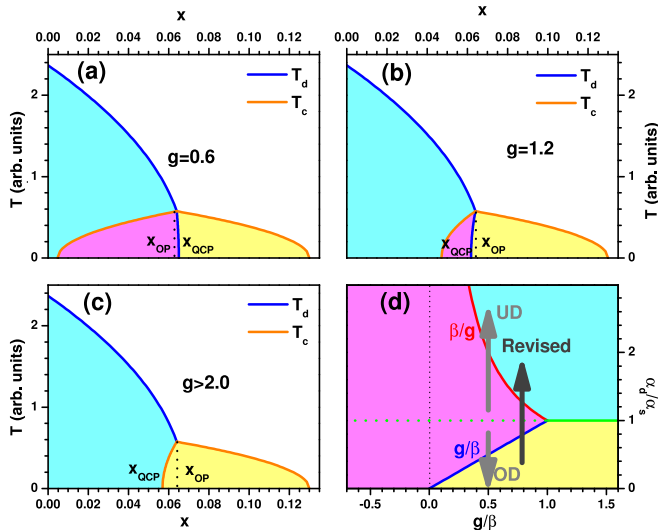


FIG. 2. Phase diagrams of the competing SC (yellow), CO (cyan), and coexisting (pink) states in Ginzburg-Landau theory using Eq. (3) for fixed $q = 0.4$. (a) The original type, where $x_{\text{QCP}} > x_{\text{OP}}$, for $g = 0.6$. (b) The revised type, where $x_{\text{QCP}} < x_{\text{OP}}$, for $g = 1.2$. (c) Complete phase separation for $g > 2$. The other parameters are $\alpha_s(x) = 10(x - 0.13)$, $\alpha_d(x) = 65(x - 0.069)$, $\beta = 2$. (d) Phase diagram in terms of interaction $\alpha_d(x, T)/\alpha_s(x, T)$ vs g/β . The light gray, and heavy gray arrows demonstrate phase transition, which occurs in the underdoping (overdoping), and in the intermediate doping region of revised phase diagram, respectively.

for $q\beta < g < \beta$ [Fig. 1(b)], providing $q < 1$ and Eq. (3). This is further shown in Fig. 2 for fixed $q = 0.4$. For strong enough competition ($g \geq \beta$), the two phases cannot coexist [Fig. 2(c)]. Therefore the original and revised types of phase diagrams can also be generated by the weak and moderate competition between SC and other COs, respectively.

To understand the relationship between q and g , we examine the phase diagram in terms of $\alpha_d(x, T)/\alpha_s(x, T)$ versus g/β using Eq. (3) [see Fig. 2(d)]. For negative g , the coexistence of SC and CO is the only solution, which means that the attractive interaction can generate neither the original nor the revised type of the phase diagrams found in high- T_c superconductors. On the other hand, for strong competing interaction $g > \beta$, the two orders cannot coexist and the phase boundary is determined by $\alpha_d(x, T)/\alpha_s(x, T) = 1$. For $0 < g < \beta$, there are two phase boundaries in Fig. 2(d). The first one between the coexisting (pink) and CO (cyan) phases is set by $\alpha_d(x, T)/\alpha_s(x, T) = \beta/g > 1$, and the second one between the SC (yellow) and coexisting (pink) phases is set by $\alpha_d(x, T)/\alpha_s(x, T) = g/\beta < 1$. When $q = 1$, the value of $\alpha_d(x, T)/\alpha_s(x, T)$ will increase as T goes up if $\alpha_d(x, 0)/\alpha_s(x, 0) > 1$, inducing the transition across the first phase boundary, as indicated by the upper gray arrow in Fig. 2(d). This corresponds to the underdoping scenario in the original phase diagram. Likewise when $q = 1$, the value of $\alpha_d(x, T)/\alpha_s(x, T)$ will decrease as T goes up if $\alpha_d(x, 0)/\alpha_s(x, 0) < 1$, inducing the transition across the second phase boundary, as indicated by the lower gray arrow in Fig. 2(d). This corresponds to the overdoping scenario in the original phase diagram. To produce the revised phase diagram

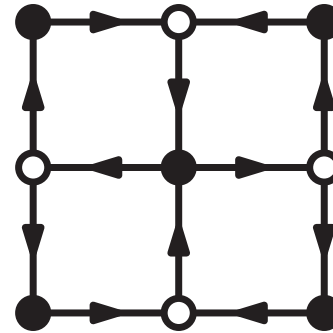


FIG. 3. Schematic of the DDW order. Solid and hollow circles are for the A and B sublattice, respectively. Signs of the DDW orders are denoted by the arrows as described in the Appendix.

where the phase undergoes pure SC, coexisting, and pseudogap state as T goes up, it requires that $\alpha_d(x, T)/\alpha_s(x, T)$ increases from smaller than g/β to larger than β/g , as indicated by the black arrow in Fig. 2(d). Such behavior can be produced only by $q < g/\beta < 1$.

We also fit the phase diagram in Ba-122 iron-pnictide though many properties of iron-based compounds differ from cuprates. However, the observed phase diagram of Ba-122 iron-pnictides [43] suggests a linear T dependence of $\alpha_d(x, T)$. Indeed, Eq. (3) does not fit quite well [Fig. 1(c)] and a better fit [Fig. 1(d)] results from using

$$\begin{aligned} \alpha_s(x, T) &= \alpha_s(x) + \frac{1-p}{\sqrt{1+p}} \sqrt{-2\alpha_s(x)\beta} T + \frac{2p}{1+p} \beta T^2, \\ \alpha_d(x, T) &= \alpha_d(x) + q\beta T, \end{aligned} \quad (4)$$

by which $\alpha_s(x, T) \simeq 2\beta T_c(T - T_c)$ near T_c is still satisfied for $0 \leq p < 1$. Here, $T_c = \sqrt{(1+p)/2} \sqrt{-\alpha_s(x)/\beta}$ in case of decoupling, similar to the form with the quadric T dependence. This revised phase diagram also resembles the recently discovered phase diagram in Bi-2212 cuprates [41,42], suggesting a possible linear T dependence of pseudogap in cuprate superconductors.

III. MICROSCOPIC DESCRIPTION IN THE EXTENDED t - J - V MODEL

We proceed to study how the revised phase diagram can emerge in a microscopic theory. We focus on the t - J -type model, which was widely used to describe the low-energy physics of the cuprates [4]. In particular, we examine the competition between SC and DDW/SDW. The commensurate DDW state (see Fig. 3) or incommensurate DDW state were shown to be the leading possible charge instability in some theories for the extended t - J - V model, where V is the nearest-neighbor Coulomb interaction [22–27,61,62]. V is known to stabilize the DDW state with respect to phase separation [26]. Following the knowledge gained from the above Ginzburg-Landau theory, we also include the V term to tune the robustness of the COs and the interaction strength between different orders. V is chosen to reproduce the qualitative phase diagram in cuprates and its magnitude is in the same order as reported in first-principle studies of cuprates [63]. Considerable V can originate from three sources, which

will be discussed later in Sec. VI. The extended t - J - V model reads

$$\mathcal{H} = - \sum_{i,j,\sigma} t_{ij} c_{i\sigma}^\dagger c_{j\sigma} + J \sum_{(i,j)} \left(\vec{S}_i \cdot \vec{S}_j - \frac{1}{4} n_i n_j \right) - \mu \sum_i n_i + V \sum_{(i,j)} n_i n_j, \quad (5)$$

where $c_{i\sigma}^\dagger$ and $c_{i\sigma}$ are electron creation and annihilation operators, respectively, at the i th lattice site with the constraint of single occupation. t_{ij} is the hopping integral between the i th and j th sites. J is the antiferromagnetic superexchange coupling constant between nearest-neighbor spins. We also consider the first, second, and third nearest-neighbor hopping integrals (t , t' , and t'' , respectively) for t_{ij} to tune the shape of the Fermi surface, which is a fundamental microscopic factor underlying the phase competition.

We introduce the mean-field order parameters as $\langle c_i^\dagger c_j \rangle = \chi \pm iD$ and $\frac{1}{2} \langle c_{i\uparrow} c_{j\downarrow} - c_{i\downarrow} c_{j\uparrow} \rangle = \pm \Delta$ with χ , D , and Δ are the uniform bond, DDW, and d -wave SC order, respectively (see Appendix for details). For simplicity, we adopt the slave-boson method [23], which directly projects the original Hamiltonian into the single occupation space via reducing the hopping terms by a factor of x . The order parameters can be self-consistently determined by minimizing the free energy

$$F = -\frac{2T}{N} \sum_{k,\eta=\pm} \ln \left(2 \cosh \frac{\beta E_k^\eta}{2} \right) - \mu(1-x) + (4V_d \chi^2 + 4V_d D^2 + 4V_c \Delta^2) \quad (6)$$

with

$$\begin{aligned} V_d &= \frac{1}{2} J + V, \\ V_c &= J - V. \end{aligned} \quad (7)$$

Here, $E_k^\pm = \sqrt{\xi_k^{\pm 2} + \Delta_k^2}$ is the Bogliubov quasiparticle dispersion in momentum space, and

$$\begin{aligned} \Delta_k &= 2V_c \Delta (\cos k_x - \cos k_y), \\ D_k &= 2V_d D (\cos k_x - \cos k_y). \end{aligned} \quad (8)$$

t has been set as the energy unit. Here we use D_k to stand for the pseudogap and the DDW critical temperature T_d for T^* .

Similar to the above macroscopic study, a revised phase diagram in hole-doped cuprates is well established within the present microscopic model. We define an intermediate doping region ranging from x_{QCP} to x_{OP} [$0.135 < x < 0.165$ in Fig 4(a)], where the back-bending of T_d under the T_c dome is found. The ground state is a pure SC state. As T increases, the coexistence of the SC and DDW states emerges when the SC order parameter is sufficiently suppressed at T_d , which is below the T_c dome. The magnitudes of the DDW and SC gaps are comparable in this special region. Our theoretical phase diagram qualitatively agrees with the recent laser-ARPES measurements on Bi-2212 and may also explain the discrepancy of x_{QCP} extrapolated by various measurements [41,42].

The T_d back-bending suggests that the role of SC in the intermediate doping region has been underestimated for

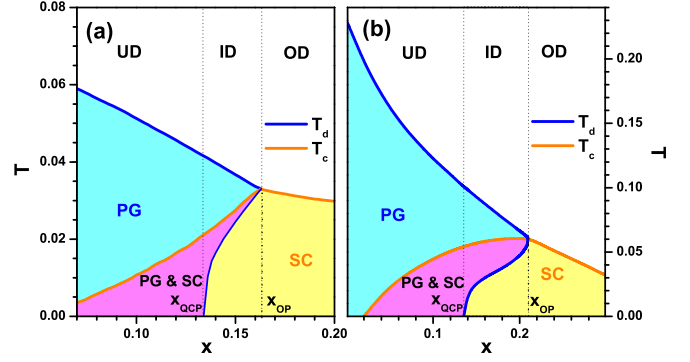


FIG. 4. Phase diagram of the extended t - J - V model in the color codes of yellow (SC), cyan (DDW), pink (coexisting). (a) Results in the slave-boson approximation for $t' = -0.25$, $t'' = 0.1$, $J = 0.35$, and $V = 0.12$; (b) Results in the renormalized mean-field theory approximation for $t' = -0.2$, $t'' = 0.1$, $J = 0.3$, and $V = 0.095$. Besides the conventional underdoping (UD) and overdoping (OD) region, an intermediate doping (ID) region where the back-bending of T_d occurs is marked out.

decades. In Fig. 4(b), we show the phase diagram in the renormalized mean-field approximation, which takes into account the feedback effect of SC for the renormalization of the model parameters [64,65] (see Appendix 2). A similar back-bending phenomenon and revised diagram are obtained, indicating that the revised phase diagram is quite robust against the theoretical approximation we chose. Moreover, the DDW enters the T_c dome now at slightly overdoping, in better agreement with experiments on Bi-2212 cuprates [41,42]. This suggests that the feedback effect of SC be necessary to quantitative explanation of the experimental data.

Figure 5 shows that the presence of the T_d back-bending is qualitatively robust against the variations in the model parameters, viz. t , t' , t'' , J , and V . According to Eq. (7), V directly enhances the DDW order parameter and weakens SC; DDW emerges at low doping for $V > J/4$. Indeed, the calculated maximum T_c decreases as V increases (see the four top panels of Fig. 5). $x_{\text{OP}} - x_{\text{QCP}}$ remains nearly unchanged for small V up to 0.135 (where the maximum T_c drops by half); then, it decreases as V increases. This behavior is different from the g or q effect shown in Ginzburg-Landau theory and is attributed to the direct tuning of $\alpha_{s,d}(x, T)$ by V . Figure 5(bottom) shows that the back-bending weakens as t' increases from a negative value (which means hole doping) to a positive one (which means electron doping), while the maximum T_c remains nearly unchanged. Thus the revised phase diagram could also appear in the electron-doped cuprates but it is more difficult to be detected.

A mean-field-type theory of the t - J - V model with $t' = 0$ [26,27] predicted a “pre-back-bending” of T_d in the absence of SC. This behavior is reproduced in our calculations for $t' = 0$, as shown in Fig. 6(a) for the decoupled SC and DDW orders. We further found that the coupling of the SC and DDW orders suppresses the back-bending for $t' = 0$, as shown in Fig. 6(c). The pre-back-bending is almost entirely removed by inclusion of $t' = -0.35$ [Fig. 6(b)]. In this case, the coupling of the SC and DDW orders drives the back-bending of T_d [Fig. 6(d)].

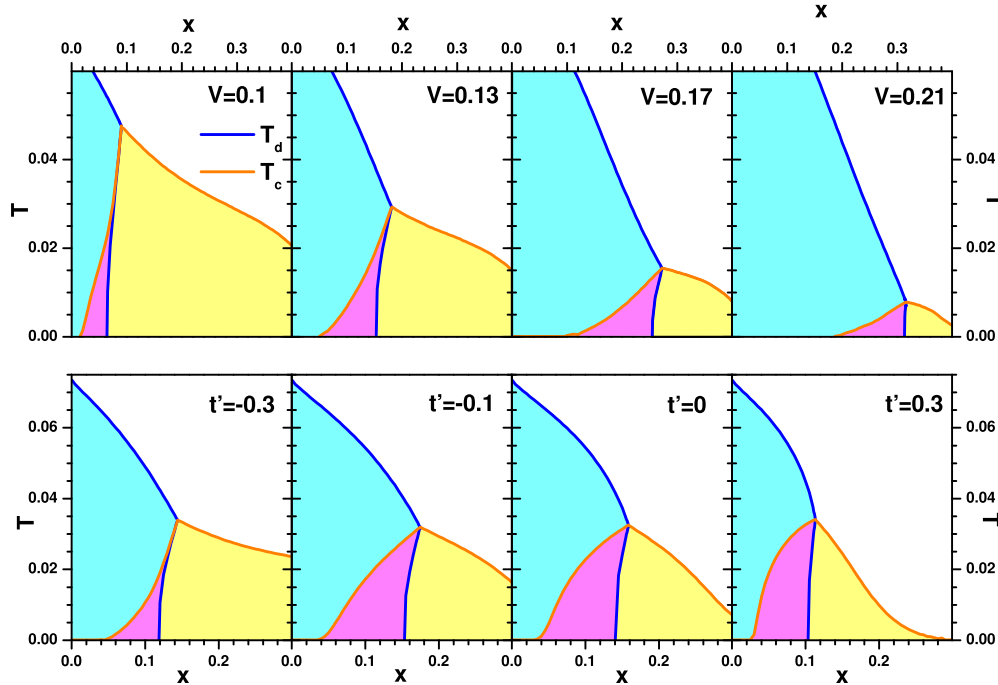


FIG. 5. Model parameter dependence of the phase diagram in the color codes of yellow (SC), cyan (DDW), pink (coexisting). (Top) The V dependence for $t' = -0.25$. (Bottom) The t' dependence for $V = 0.12$. $t'' = 0.1$ and $J = 0.35$ for all the figures.

Whether the back-bending occurs above the T_c dome for $t' = 0$ [26], as shown in Fig. 6(c), depends on the model parameters. For a smaller V , the back-bending starts right at T_c for $t' = 0$ [see Fig. 7(c)], while the other features of Fig. 6 remain unchanged in Fig. 7.

Incommensurate DDW. It is previously reported that for $t = 0$, the pre-back-bending of T_d in the absence of SC vanishes upon inclusion of the incommensurate DDW, yielding a continuous decreasing of T_d upon doping [27]. We also

check whether the back-bending is suppressed by the incommensurate DDW. To determine the phase boundary of the incommensurate DDW state, we study the charge instability under the random phase approximation (RPA) (see Appendix for details).

The pre-back-bending in the normal state is removed when the incommensurate DDW is further considered as shown in Fig. 6(a) where only the nearest-neighbor hopping is considered, consisting with the previous results obtained by

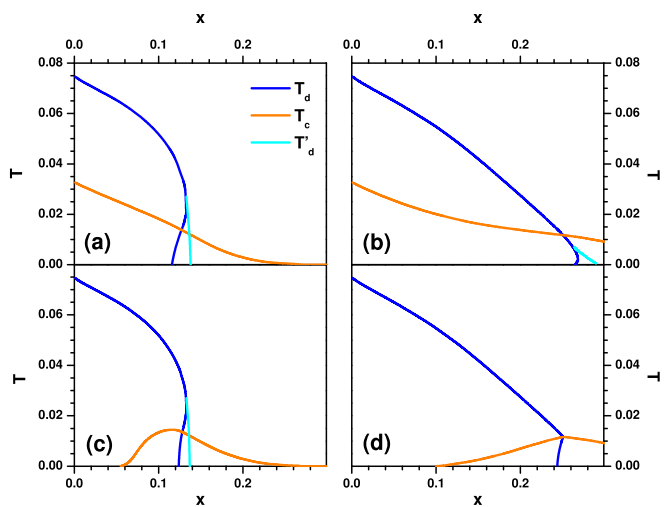


FIG. 6. The effects of t' on the pre-back-bending of T_d in the extended t - J - V model. The DDW and SC orders are decoupled for (a) $t' = 0$ and (b) $t' = -0.35$. They are coupled for (c) $t' = 0$ and (d) $t' = -0.35$. T'_d is the characteristic temperature for the incommensurate DDW as discussed in main text. $t'' = 0$, $J = 0.3$, and $V = 0.15$ for all.

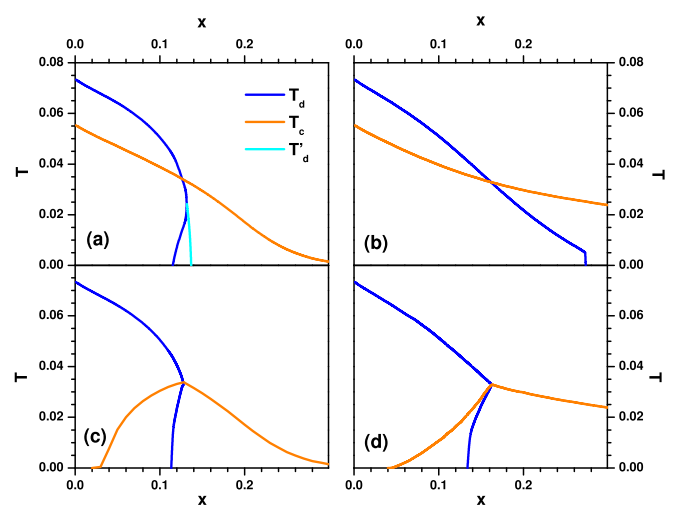


FIG. 7. The effects of t' on the pre-back-bending of T_d in the extended t - J - V model. The DDW and SC orders are decoupled for (a) $t' = 0$ and (b) $t' = -0.25$. They are coupled for (c) $t' = 0$ and (d) $t' = -0.25$. T'_d is the characteristic temperature for the incommensurate DDW as discussed in main text. $t'' = 0.1$. $J = 0.35$, and $V = 0.12$ for all.

large- N expansion method [27]. Such an incommensurate DDW state remains for weak SC [Fig. 6(c)]. However, the incommensurate DDW is strongly suppressed by the next nearest-neighbor hopping t' as shown in Fig. 6(b). Furthermore, the incommensurate DDW state is also suppressed by strong SC [Figs. 6(d) and 7(c)]. Especially, the incommensurate DDW state is fully suppressed for the realistic parameters [Figs. 7(b) and 7(d)]. Therefore the back-bending of T_d under T_c dome presented here is driven by the interplay of SC and commensurate DDW. However, the back-bending phenomenology is parameter dependent, which may be the reason why its manifestation is found only in limited cuprates.

IV. ANOMALOUS THERMAL EVOLUTION OF ELECTRONIC SPECTRAL FEATURES

To explore whether and how the revised phase diagram is related to the observed anomalous temperature dependence of the antinodal gap and Raman response, we calculate these quantities in the microscopic theory.

A. The quasiparticle spectral functions

First, we focus on the SC and DDW order parameters Δ_k and D_k [see Eq. (8)] and the quasiparticle spectral functions, which are the observable in ARPES measurements. Figure 8 shows the results at $\mathbf{k} = (k_f, 0)$, the normal-state Fermi-surface momentum along the antinodal line, for three typical doping levels. For underdoping $x < 0.13$ [Fig. 8(a)], the magnitude of the “pseudogap” D_k is much larger than that of the SC gap Δ_k . Δ_k decreases but D_k increases as temperature increases for $T < T_c$. On the other hand, the gaps evaluated from the spectral functions (see Appendix) differ from the two order parameters. There exist two peaks with different weight factors below the Fermi level [cf. Fig. 8(d)]; the one with substantially stronger intensity used to represent the measured gap. In the underdoped region, the high-energy peak (HEP) has much stronger intensity than the low-energy peak (LEP) and remains nearly unchanged below T_c . This reflects the fact that pseudogap dominates the underdoping region. In the overdoping region, the temperature dependence of gap follows the traditional BCS behavior since the pseudogap is absent [Fig. 8(b)]. These findings agree with our common knowledge and various ARPES measurements [50].

On the contrary, in the intermediate doping range [Fig. 8(c)], the “pseudogap” D_k does not emerge unless the SC gap Δ_k is suppressed sufficiently at T_d , similar to the previous theoretical suggestions [66–68]. On the other hand, the measured gap exhibits a pronounced two-step evolution. It evolves from the SC dominating at low temperature to the DDW dominating at high temperature [Figs. 8(c) and 8(d)]. The most important feature is that the measured gap exhibits clear enhancement as temperature increases above T_d (under the T_c dome), especially for slight underdoping. Therefore we find a special temperature region in the intermediate doping region where the measured gap shows anomalous temperature dependence, in good agreement with ARPES measurements on various families of cuprates [47–50]. The present explanation also differs from the previous illustrations that attribute the anomalous temperature dependence of the measured antinodal

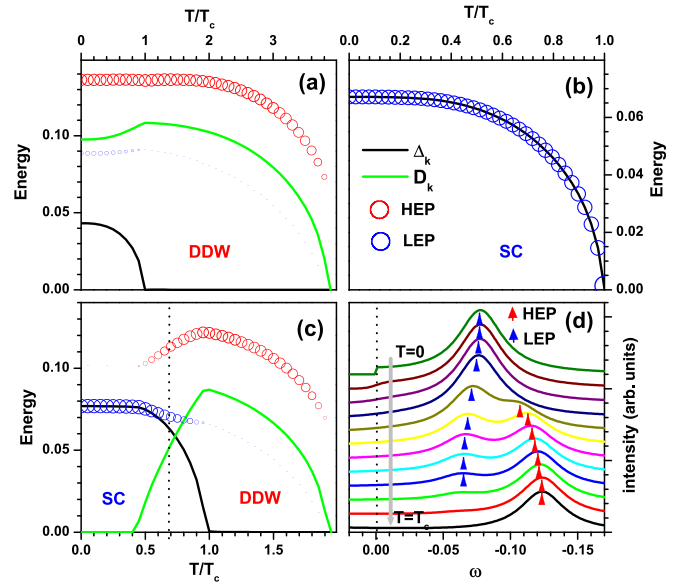


FIG. 8. Thermal evolution of the SC and DDW order parameters and measured antinodal gap for three distinct doping levels: (a) underdoping $x = 0.11$, (b) overdoping $x = 0.18$, and (c) intermediate doping $x = 0.135$. The legends of SC and DDW indicate the SC- and DDW-dominated regions, respectively. Solid lines are for the SC (black) and DDW (green) order parameters at the Fermi surface along the antinodal line. The open circles are for the peak energies extracted from the spectral functions; HEP and LEP stand for the high- and low-energy peaks, respectively. The size of the circles scales with the peak intensity. (d) Temperature evolution of the spectral functions at the intermediate doping $x = 0.135$. The peak positions are marked by triangles with red for HEP and blue for LEP. The model parameters are $t' = -0.25$, $t'' = 0.1$, $J = 0.35$, and $V = 0.12$. The Fermi energy is fixed at 0.

gap to either the Fermi function [69] or the weakened SC gap [70]. Our results show that the SC gap near the borderline between the SC- and DDW-dominated regions [dotted line in Fig. 8(c)] only slightly weakens, in agreement with the ARPES measurements on near optimally doped Bi-2212 [42].

We noted that the measured gap remains increasing even above T_c as revealed by ARPES data [50]. This may be due to the pre-pairing of superconductivity. Although the superconducting gap and pseudogap come from different origin, the electrons may have been paired above T_c as indicated by the ARPES [47] and other experimental measurements [71–73]. Therefore the back-bending phenomenon, and the region of intermediate doping, is expected to be more pronounced due to strong superconducting gap magnitude.

B. The Raman response

Furthermore, we study the relationship between the revised phase diagram and the anomalous temperature dependence of ERS in the cuprates. The Raman response was calculated from using the density-density correlation function (see Appendix). The B_{1g} and B_{2g} channels are contributed mainly from the Fermi surface around the antinodal and nodal regions, respectively [53,54]. The peak energy corresponding to the B_{2g} response was found to track the temperature evolution of

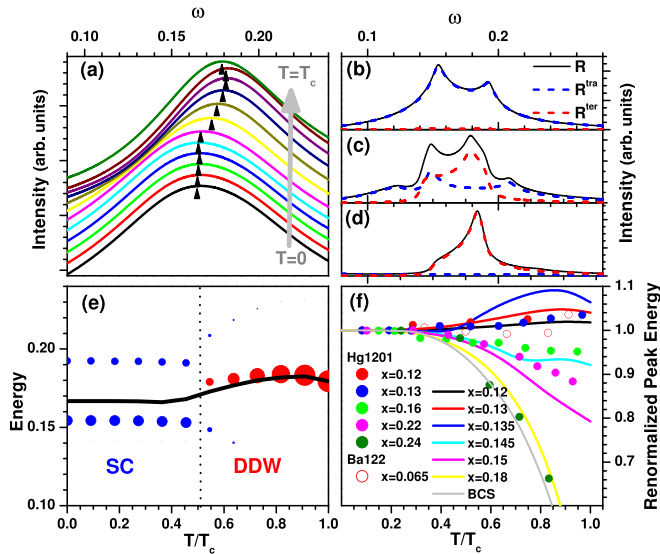


FIG. 9. Thermal evolution of the Raman response in the B_{1g} channel at intermediate doping $x = 0.135$. (a) The results for the broadened resolution of $\eta = 0.04$. The peak positions are indicated by the triangles. (b)–(d) is Raman response at three typical temperature with high resolution $\eta = 0.003$. $T = 0.3T_c$ for (b), $T = 0.7T_c$ for (c), and $T = 0.9T_c$ for (d). The intraband and interband components R^{tra} and R^{ter} is denoted by blue, and red dashed lines, respectively. R is the sum of R^{tra} and R^{ter} denoted by solid black line. (e) Temperature dependence of the energy of B_{1g} Raman response peak. The circles track the peak energy shown (b)–(d) with high resolution, the intensity is marked by size. The solid line is the peak energy with broadened resolution extracted from (a). SC and DDW denote the SC- and DDW-dominated regions, respectively, as described in text. (f) Theoretical results under broadened resolution at different doping, together with the experimental Raman data in cuprate Hg-1201 [53,54] and near optimally doped iron-pnictide Ba-122 [59]. $t' = -0.25$, $t'' = 0.1$, $J = 0.35$, and $V = 0.12$.

the d -wave SC order due to the absence of pseudogap near the nodal region.

On the other hand, the Raman response in the B_{1g} channel is much more complicated. In the underdoped region, the peak energy in the Raman response remains nearly unchanged with increasing temperature. It decreases monotonically with temperature and goes to zero at T_c in the overdoping region, following a simple BCS-like temperature evolution. On the contrary, the peak energy of the Raman response in the intermediate doping region [Fig. 9(a)] clearly enhances upon increasing temperature toward T_c . These behaviors are qualitatively consistent with our calculated temperature dependence of the measured quasiparticle gap and the ERS measurements [53–55], where a slight upward shift of the antinodal gap component was detected in the slightly underdoped Hg1201 and Bi2212 as T_c is approached. The discrepancy in the temperature evolution of the B_{1g} and B_{2g} ERS would favor the two-gap scenario.

The above single peak was obtained from using the broadened resolution of $\eta = 0.04$. It is resolved into multi-peaks with $\eta = 0.003$ owing to the intraband (blue) and interband (red) contributions [Figs. 9(b)–9(d)]. At low temperature ($T \ll T_c$)

where SC dominates [Fig. 9(b)], the Raman response comes from the intraband scattering due to the near degeneracy of the lower and upper bands. Two peaks can be found: the high-energy one originates from Van Hove singularity [74] and the low-energy one from the SC gap opening along the Fermi surface. At intermediate temperature [Fig. 9(c)], both SC and DDW orders play significant roles. Apart from the intraband contribution, the interband contribution, which is dominated by DDW, develops gradually. At high enough temperature where DDW dominates [Fig. 9(d)], the interband contribution takes over and the intraband contribution is invisible. In Fig. 9(e), we combine the information about the peak positions and the peak intensities as a function of temperature. It is clear that the temperature evolution of Raman response exhibits a two-step pattern with an anomalous enhancement near the transition from the SC-dominated region to the DDW-dominated region.

To complete, in the heavily overdoped region, the Raman peak energy follows the BCS prediction and decreases to zero as T approaches T_c . The above results qualitatively agree with the experimental data on HgBa₂CuO_{4+ δ} (Hg-1201) [53–55], as summarized in Fig. 9(f).

Most importantly, we found that the anomalous temperature enhancement of the peak energy in the B_{1g} Raman response as $T \rightarrow T_c$ near x_{QCP} is intimately related to the back-bending of T_d below the T_c dome. It is nearly invisible for weak back-bending of T_d and disappears in the original phase diagram. This may suggest the possible existence of the revised phase diagram in Hg-1201 where the anomalous temperature dependence of ESR peak energy is detected.

V. SPIN-DENSITY WAVE AS A COMPETING ORDER

We have presented the results for the CO being DDW, which has the d -wave symmetry. We also considered the competition between the SC and an s -wave-like order such as SDW. Unlike DDW, the SDW order can be stabilized at low doping for $V = 0$. Increasing V will once again suppress the SC dome according to Eq. (7), as shown in Fig. 10.

Figure 11(a) presents a revised phase diagram that looks similar to the case of DDW as a CO. However, the SDW case exhibits considerably weakened T_d back-bending under the T_c dome in the intermediate doping range. The back-bending even disappears for certain parameters, giving rise to an original phase diagram. Meanwhile, the anomalous thermal evolution in the measured antinodal gap and in B_{1g} Raman channel is also suppressed [Fig. 11(b)], consisting with the results found in DDW case. This may be understood as the case that DDW competes with SC more fiercely than SDW in the antinodal region. Hence the pseudogap in the hole-doped cuprates is more likely to be a manifestation of DDW than SDW based on the mean-field theory, although it should be attested by rigorous numerical techniques.

VI. DISCUSSION

In the Landau theory, the revised and original phase diagrams in high- T_c superconductors can be established with

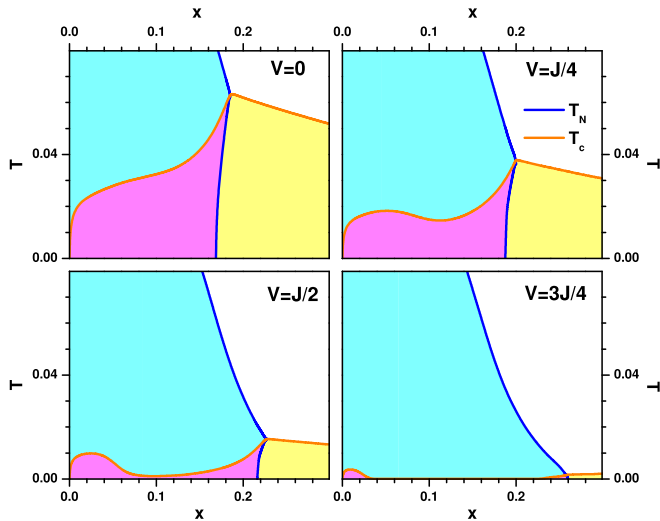


FIG. 10. The V dependence of the phase diagram in the color codes of yellow (SC), cyan (SDW), pink (coexisting) for $t' = -0.25$, $t'' = 0.1$, and $J = 0.35$.

the moderate and weak competitions, respectively. Thus the question turns out to be whether the revised phase diagram does take place in real materials. In the basic t - J model for cuprate superconductors, the pairing gap increases as the doping level decreases, promoting the notions of the pseudogap as a manifestation of preformed pairs and the T_c dome as a manifestation of superconducting phase decoherence at low doping [16–19]. Inclusion of the nearest-neighbor Coulomb interaction V favors DDW as the pseudogap state against SC in the underdoped region, leading to the formation of the T_c dome structure in the phase diagram [22–27]. There are three possible sources for considerable V : (i) strongly correlated metals are generally bad metals with large resistivity of the order of $\text{m}\Omega \cdot \text{cm}$ and small optical Drude peak. Therefore the electrostatic screening does not work well in those systems [14,75–78]. (ii) In mean-field theory, the local constraint of no-double occupancy at each site is reinforced only globally. As a result, the expectation value of $\langle n_i n_j \rangle$

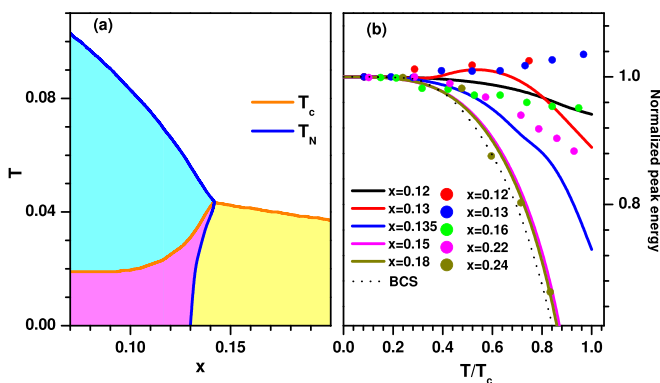


FIG. 11. (a) Phase diagram and (b) Raman response in the extended t - J - V model with an s -wave-like pseudogap SDW instead of the d -wave-like DDW. Symbols in (b) are experimental data extracted from cuprates Hg_{1201} [53,54]. $t' = -0.25$, $t'' = 0.1$, $J = 0.25$, and $V = 0$.

is substantially greater than one for the undoped case. In this sense, V acts to minimize this side effect of mean-field theory. (iii) More interestingly, upon mapping multi-orbital real materials into a one-band effective low-energy Hamiltonian, a vacuum-fluctuation-induced effective interaction in the exactly same form as V appears together with J [63,79]. Like the superexchange J term, the new “super-repulsion” V term comes from virtual electron-hopping processes, which can hardly be screened electrostatically. The strength of super-repulsion V is strongly material dependent, since the apical atoms are involved in the intermediate state of the vacuum charge fluctuation: V/t was estimated to be 0.28, 0.12, and 0.08 for apical oxygen (in La_2CuO_4), chlorine (in $\text{Sr}_2\text{CuO}_2\text{Cl}_2$), and fluorine (in $\text{Sr}_2\text{CuO}_2\text{F}_2$), respectively [63]. Our present calculations using this range of V yield a revised phase diagram and electronic spectra consistent with ARPES and ERS measurements, indeed. Moreover, the realistic value of $t' \sim -0.3$ is found to remove the pre-back-bending of T_d . Thus it is necessary to include V and t' in addressing the phase diagram of the real cuprate materials. The strong material dependence of V renders the stability of DDW to be a material specific issue.

Following the above argument, V in terms of effective low-energy Hamiltonian should be considerably strong in correlated electron systems in general. Like in the cuprates, V may promote charge instabilities in the iron-based superconductors [78] in competition with SC. We notice that similar anomalous temperature dependence of ERS in the B_{2g} channel was discovered in slightly underdoped Ba-122 iron-based superconductor [59] [open circles in Fig. 9(f)]. Together with the similar phase diagrams [Figs. 1(c) and 1(d)], this suggests the existence of strong competition between superconductivity and competing orders in iron-pnictide high- T_c superconductors. Although the cuprates and iron pnictides appear very different from each other, e.g., in the properties of their parent materials, Fermi surface topology, forms of interactions, etc., they both exhibit strong phase competition. In fact, the active orbital physics in iron pnictides make the C_2 and C_4 competition more apparent in K-doped BaFe_2As_2 or Na-doped SrFe_2As_2 [80–84].

It is noteworthy that the present work has focused on the competition between SC and DDW/SDW. DDW was shown to be the leading possible charge instability in the one-band t - t' - J - V model [27]. The recent Hall effect measurements on $\text{YBa}_2\text{Cu}_3\text{O}_y$ conducted at strong magnetic fields up to 88 tesla to suppress SC suggest that the pseudogap phase is disconnected from the charge-density wave (CDW) observed in the underdoped regime but linked to the antiferromagnetic Mott insulator [6]. This is not inconsistent with the DDW scenario, as DDW is not an ordinary CDW state whose order parameter is proportional to $\langle c_i^\dagger c_i \rangle$ or real $\langle c_i^\dagger c_j \rangle$ driven by Fermi surface instability, but a flux or bond-charge-phase order in terms of complex $\langle c_i^\dagger c_j \rangle$ due to the Mottness. For some other well-known COs such as loop-current order [32] and intraunit-cell nematic orders [35], the three-band Emery model is an appropriate starting point. And it is yet to be seen whether the competition between SC and any other CO can produce a revised phase diagram and electronic spectra consistent with ARPES and ERS measurements in a realistic microscopic model.

VII. SUMMARY

We have shown in Ginzburg-Landau theory that the revised and original phase diagrams in high- T_c superconductors can be established with the moderate and weak phase competitions, respectively. We further show that the revised phase diagram can result from the competition between DDW and SC or between SDW and SC in mean-field theory of the realistic t - t' - t'' - J - V model. Inclusion of the much neglected feedback effect of SC on pseudogap can push the back-bending point from optimal doping to the overdoped regime. The calculated ARPES and ERS spectral functions reveal that the back-bending of T^* can give a simple explanation of the observed anomalous temperature dependence of the antinodal gap via a two-step evolution where the SC and DDW dominate low- and high-temperature regions, respectively. Our results imply that it is likely to realize the revised phase diagram in cuprate superconductors.

ACKNOWLEDGMENTS

We thank P. D. Johnson, J.-X. Li, and Z.-X. Shen for helpful discussions and suggestions. This work was supported by the National Nature Science Foundation of China under Contract No. 11274276, the Ministry of Science and Technology of China 2016YFA0300401, and the U.S. Department of Energy (DOE), Office of Basic Energy Science, under Contract No. DE-SC0012704. Y.Z. acknowledges the financial support of CSC and visiting scholarship of Brookhaven National Laboratory. H.-Q.L. acknowledges support from NSAF U1530401 and computational resource from the Beijing Computational Science Research Center.

APPENDIX: SOLVING THE EXTENDED t - J - V MODEL

The extended t - J - V model is solved in mean-field-type theories with the order parameters defined as follows. (i) The d -wave SC order $\frac{1}{2}(c_{i\uparrow}c_{j\downarrow} - c_{i\downarrow}c_{j\uparrow}) = \pm\Delta$ with $+$ for the x direction and $-$ for the y direction, (ii) the uniform bond order and the DDW order $\langle c_i^\dagger c_j \rangle = \chi \pm iD$ with $+$ for the x direction of the A sublattice and the y -direction of the B sublattice, and $-$ otherwise (see Fig. 3), and (iii) the SDW order $\frac{1}{2}(c_{i\uparrow}^\dagger c_{i\uparrow} - c_{i\downarrow}^\dagger c_{i\downarrow}) = (-1)^i m$. The interacting terms $H_{JV} = J \sum_{\langle i,j \rangle} (\vec{S}_i \cdot \vec{S}_j - \frac{1}{4} n_i n_j) + V \sum_{\langle i,j \rangle} n_i n_j$ are decoupled into the particle-particle and particle-hole channels [23]:

$$\begin{aligned} H_{JV} = & -V_c \sum_{\langle i,j \rangle} [\Delta(c_{i\downarrow}^\dagger c_{j\uparrow}^\dagger - c_{j\downarrow}^\dagger c_{i\uparrow}^\dagger) + \text{H.c.}] \\ & - V_d \sum_{\langle i,j \rangle} [(\chi \pm iD)(c_{j\uparrow}^\dagger c_{i\uparrow} + c_{j\downarrow}^\dagger c_{i\downarrow}) + \text{H.c.}] \\ & + 2Jm \sum_i (-1)^i (c_{i\uparrow}^\dagger c_{i\uparrow} - c_{i\downarrow}^\dagger c_{i\downarrow}), \end{aligned} \quad (\text{A1})$$

where $V_c = J - V$ and $V_d = J/2 + V$.

1. Slave-boson approximation

In the slave-boson approximation, the physical electron operators $c_{i\sigma} = b_i^\dagger f_{i\sigma}$ are represented by slave bosons b_i carrying the charge and fermions $f_{i\sigma}$ representing the spin σ

with the constraint $\sum_\sigma f_{i\sigma}^\dagger f_{i\sigma} + b_i^\dagger b_i = 1$ [85]. In mean-field theory, bosons condense $b_i \rightarrow \langle b_i \rangle = \sqrt{x}$ with x the hole concentration. The mean-field Hamiltonian is then expressed in momentum space as

$$H = \sum_k \psi_k^\dagger \begin{pmatrix} \varepsilon_k & -iD_k & \Delta_k & 0 \\ iD_k & \varepsilon_{k+Q} & 0 & -\Delta_k \\ \Delta_k & 0 & -\varepsilon_k & -iD_k \\ 0 & -\Delta_k & iD_k & -\varepsilon_{k+Q} \end{pmatrix} \psi_k, \quad (\text{A2})$$

where $\psi_k = (f_{k\uparrow} f_{k+Q\uparrow} f_{-k\downarrow}^\dagger f_{-k-Q\downarrow}^\dagger)^T$ with $Q = (\pi, \pi)$ being the antiferromagnetic wave vector. $\varepsilon_k = -2(xt + V_d\chi)(\cos k_x + \cos k_y) - 4xt' \cos k_x \cos k_y - 2xt(\cos 2k_x + \cos 2k_y) - \mu$ with t , t' , and t'' being the nearest-, next-nearest-, and third-nearest-neighbor hopping constants, respectively. $D_k = 2V_d D(\cos k_x - \cos k_y)$, and $\Delta_k = 2V_c \Delta(\cos k_x - \cos k_y)$. The summation is restricted in the magnetic Brillouin zone.

The order parameters can be self-consistently determined by minimizing the free energy

$$\begin{aligned} F = & -\frac{2T}{N} \sum_{k,\eta=\pm} \ln \left(2 \cosh \frac{\beta E_k^\eta}{2} \right) - \mu(1-x) \\ & + (4V_d\chi^2 + 4V_d D^2 + 4V_c \Delta^2). \end{aligned} \quad (\text{A3})$$

Here, $E_k^\eta = \sqrt{(\xi_k^\eta)^2 + \Delta_k^2}$ with $\xi_k^\eta = (\frac{\varepsilon_k + \varepsilon_{k+Q}}{2}) + \eta \sqrt{(\frac{\varepsilon_k - \varepsilon_{k+Q}}{2})^2 + |D_k|^2}$ ($\eta = 1$ and -1 for upper and lower band, respectively) is obtained by unitary transformation with the 4×4 matrix U_k [86].

When the incommensurate DDW order is included, the phase boundary is determined by the charge order instability under the random phase approximation (RPA). The RPA charge susceptibility for DDW is

$$\chi_{\text{RPA}}(i\nu, q) = \frac{\chi_0(i\nu, q)}{1 - (\frac{J}{4} + \frac{V}{2})\chi_0(i\nu, q)}. \quad (\text{A4})$$

Here, the bare charge susceptibility for DDW is $\chi_0(\tau, q) = \langle T \rho_q(\tau) \rho_q^\dagger(0) \rangle_0$ with $\rho_q(\tau) = \sum_{k\sigma} i(\sin(k_x - \frac{q_x}{2}) - \sin(k_y - \frac{q_y}{2})) f_{k+q\sigma}^\dagger(\tau) f_{k\sigma}(\tau)$. The charge instability is therefore judged from the divergency of the RPA charge susceptibility at zero frequency, yielding the simple criterion of $\mathcal{D}(q) = 1 - (\frac{J}{4} + \frac{V}{2})\chi_0(0, q) = 0$ with $\mathcal{D}(q)$ the denominator at zero frequency. Here, $q = (\pi, \pi - \delta q)$ with $\delta q = 0$, and $\delta q \neq 0$ for the commensurate, and incommensurate DDW, respectively.

Figure 12 shows some relevant results at low enough temperature. The data containing only the nearest-neighbor hopping are shown in Fig. 12(a). The instability of the commensurate DDW order occurs at doping density about $x = 0.123$ where $\mathcal{D}(q) = 0$ with $dq = 0$. In comparison, the incommensurate DDW instability occurs at about $x = 0.135$ with $dq \sim 0.1\pi$ [also see Fig. 6(c) in main text]. This is well consistent with the previous results obtained by large- N expansion in absence of superconductivity [27], manifesting the existence of the incommensurate DDW order. It had been shown that the incommensurate DDW order is strongly weakened by introducing the next-nearest-neighbor hopping [27] [Fig. 6(b) in main text]. Furthermore, the incommensurate

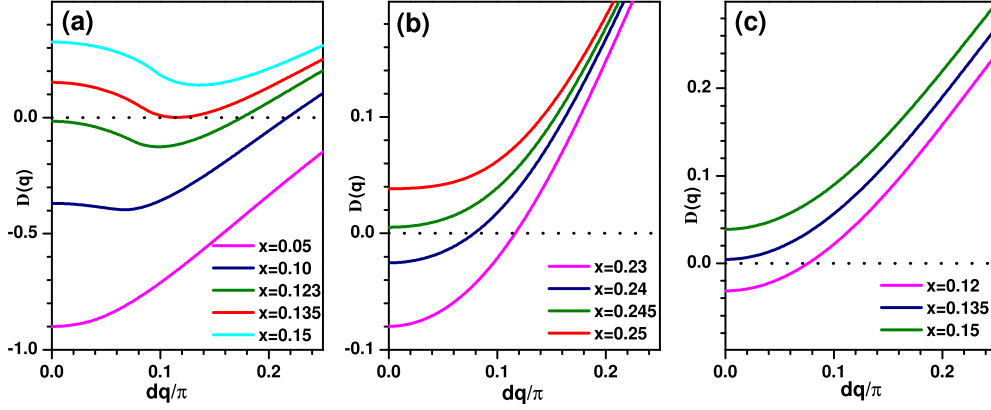


FIG. 12. (a) The denominator of RPA DDW charge susceptibility $\mathcal{D}(q)$ with different parameters. (a) $t' = 0, t'' = 0, J = 0.3$, and $V = 0.15$; (b) $t' = -0.35, t'' = 0, J = 0.3$, and $V = 0.15$; and (c) $t' = -0.25, t'' = 0.1, J = 0.3$, and $V = 0.12$. The temperature is fixed at 1×10^{-4} .

DDW order may be further suppressed by SC as shown in Fig. 12(b) [also Fig. 6(d)], no instability of the incommensurate DDW state is found when the superconductivity is included. The DDW instability in the SC state with the parameters presented in the main text is shown in Fig. 12(c), only the commensurate DDW instability occurs at about $x = 0.135$.

The spectral function $A(k, \omega) = -\frac{1}{\pi} \Im G^{11}(k, i\omega_l \rightarrow \omega + i\Gamma)$ is calculated with the Matsubara Green function

$$G^{nm}(k, i\omega_l) = \sum_{j=1}^4 (U_k)_{nj} \frac{1}{i\omega_l - E_k^j} (U_k^\dagger)_{jm}. \quad (\text{A5})$$

The Raman response is described by the following Matsubara correlation function [74]

$$R_\gamma(q, \tau) = -\langle T \rho_{\gamma_k}(q, \tau) \rho_{\gamma_k}(-q, 0) \rangle, \quad (\text{A6})$$

where $\rho_\gamma(q, \tau) = \sum_k f_{k+q/2}^\dagger(\tau) \gamma_k f_{k-q/2}(\tau)$ with the vertex $\gamma_k = \frac{1}{2} \left(\frac{\partial^2 \varepsilon_k}{\partial k_x^2} - \frac{\partial^2 \varepsilon_k}{\partial k_y^2} \right)$ for the B_{1g} channel and $\gamma_k = \frac{\partial^2 \varepsilon_k}{\partial k_x \partial k_y}$ for the B_{2g} channel. At the zero-momentum transfer, $R_\gamma(0, i\omega_l)$ corresponds to what ERS experiments measure

$$R_\gamma(0, i\omega_l) = \sum_{k,n,m} \frac{f(E_k^n) - f(E_k^m)}{i\omega_l + E_k^m - E_k^n} |(U_k^\dagger \gamma_k U_k)_{nm}|^2 \quad (\text{A7})$$

with $f(E_k^n)$ the Fermi-Dirac function.

2. Renormalized mean-field theory

The renormalized mean-field theory (RMFT) projects the Hamiltonian by Gutzwiller factors. The expectation value of the projected Hamiltonian is

$$\begin{aligned} \langle H \rangle = & - \sum_{ij\sigma} g^t t_{ij} \langle \chi + iD \rangle - \mu \sum_{i\sigma} \langle n_\sigma \rangle \\ & - 2 \left[\left(\frac{1}{2} g^{xy} + \frac{1}{4} g^z \right) J - V \right] \sum_{(i,j)} \langle \Delta \rangle \langle \Delta \rangle^* \end{aligned}$$

$$\begin{aligned} & - 2 \left[\left(\frac{1}{2} g^{xy} + \frac{1}{4} g^z \right) J + V \right] \sum_{(i,j)} (\chi + iD)^* (\chi + iD) \\ & + g^z J \sum_{(i,j)} \langle m_i \rangle \langle m_j \rangle, \end{aligned} \quad (\text{A8})$$

where χ , D , Δ , and m are variational parameters (their sign rules are the same as those specified in the last subsection). g^t , g^{xy} , g^z are the Gutzwiller factors for hopping, transverse and longitudinal spin-exchange terms, respectively. The expectation value of an operator O in the projected state is $g^O \langle O \rangle$ with $\langle O \rangle$ is the expectation value in the unprojected state and g^O is the Gutzwiller factor for operator O . Here, $g^\Delta = (g^t)^2$, $g^m = \sqrt{g^z}$, $g^{\chi \cdot D} = g^t$.

In fact, the simplest Gutzwiller approximation [17] does not reproduce the results obtained by variational Monte Carlo method. For example, the resulting antiferromagnetic state extends to high doping density. It can be improved by taking the feedback effect of the order parameters into account [64,87]. The modified Gutzwiller factors are

$$g^t(i, j) = \frac{2x}{1+x}, \quad g^{xy} = g^z = \left(\frac{2}{1+x} \right)^2 a^{-7}, \quad (\text{A9})$$

where $a = 1 + \frac{4X}{(1-x^2)^2}$ with $X = 2x^2(\Delta^2 - |\chi + iD|^2) + 2(|\chi + iD|^2 + \Delta^2)^2$.

At finite temperature, one should minimize the free energy $F = \langle H \rangle - TS$ instead. $\langle H \rangle$ is straightforward by using finite temperature Wicks theorem. $S = S_0 + \delta S$ with $S_0 = -\sum_n [f(E_n) \ln f(E_n) + (1-f(E_n)) \ln(1-f(E_n))]$ is the entropy in the mean-field trial state, f is the Fermi-Dirac distribution function, and δS is the entropy which losses under projection as [65]

$$\delta S = -N \left(x \ln \frac{4x}{(1+x)^2 + 4m} + (1-x) \ln \frac{2(1-x)}{1-x^2 + 4m} \right). \quad (\text{A10})$$

For the nonmagnetic case, δS is temperature independent and thus can be ignored.

- [1] E. Dagotto, *Science* **309**, 257 (2005).
- [2] J. C. S. Davis and D.-H. Lee, *Proc. Natl. Acad. Sci. USA* **110**, 17623 (2013).
- [3] E. Fradkin, S. A. Kivelson, and J. M. Tranquada, *Rev. Mod. Phys.* **87**, 457 (2015).
- [4] P. A. Lee, N. Nagaosa, and X.-G. Wen, *Rev. Mod. Phys.* **78**, 17 (2006).
- [5] Ø. Fischer, M. Kugler, I. Maggio-Aprile, C. Berthod, and C. Renner, *Rev. Mod. Phys.* **79**, 353 (2007).
- [6] S. Badoux, W. Tabis, F. Laliberté, G. Grissonnanche, B. Vignolle, D. Vignolles, J. Béard, D. A. Bonn, W. N. Hardy, R. Liang, N. Doiron-Leyraud, L. Taillefer, and C. Proust, *Nature (London)* **531**, 210 (2016).
- [7] N. Hussey, *Nat. Phys.* **12**, 290 (2016).
- [8] D. Rybicki, M. Jurkutat, S. Reichardt, C. Kapusta, and J. Haase, *Nat. Commun.* **7**, 11413 (2016).
- [9] J. R. Jeffries, N. A. Frederick, E. D. Bauer, H. Kimura, V. S. Zapf, K.-D. Hof, T. A. Sayles, and M. B. Maple, *Phys. Rev. B* **72**, 024551 (2005).
- [10] X. G. Luo, T. Wu, and X. H. Chen, in *Iron-Based Superconductivity*, edited by P. D. Johnson, G. Xu, and W.-G. Yin, Springer Series in Materials Science Vol. 211 (Springer International Publishing, New York, 2015).
- [11] C.-C. Lee, W.-G. Yin, and W. Ku, *Phys. Rev. Lett.* **103**, 267001 (2009).
- [12] S. Onari, Y. Yamakawa, and H. Kontani, *Phys. Rev. Lett.* **112**, 187001 (2014).
- [13] R. Yu and Q. Si, *Phys. Rev. Lett.* **115**, 116401 (2015).
- [14] B. A. Frandsen, E. S. Bozin, H. Hu, Y. Zhu, Y. Nozaki, H. Kageyama, Y. J. Uemura, W.-G. Yin, and S. J. L. Billinge, *Nat. Commun.* **5**, 5761 (2014).
- [15] E. Morosan, H. W. Zandbergen, B. S. Dennis, J. W. G. Bos, Y. Onose, T. Klimczuk, A. P. Ramirez, N. P. Ong, and R. J. Cava, *Nat. Phys.* **2**, 544 (2006).
- [16] P. W. Anderson, *Science* **235**, 1196 (1987).
- [17] F. C. Zhang, C. Gros, T. M. Rice, and H. Shiba, *Supercond. Sci. Technol.* **1**, 36 (1988).
- [18] G. Kotliar and J. Liu, *Phys. Rev. B* **38**, 5142 (1988).
- [19] E. J. Emery and S. A. Kivelson, *Nature (London)* **374**, 434 (1995).
- [20] M. Shi, J. Chang, S. Pailhès, M. R. Norman, J. C. Campuzano, M. Månsson, T. Claesson, O. Tjernberg, A. Bendounan, L. Patthey, N. Momono, M. Oda, M. Ido, C. Mudry, and J. Mesot, *Phys. Rev. Lett.* **101**, 047002 (2008).
- [21] A. Kanigel, U. Chatterjee, M. Randeria, M. R. Norman, G. Koren, K. Kadowaki, and J. C. Campuzano, *Phys. Rev. Lett.* **101**, 137002 (2008).
- [22] S. Chakravarty, R. B. Laughlin, D. K. Morr, and C. Nayak, *Phys. Rev. B* **63**, 094503 (2001).
- [23] M. U. Ubbens and P. A. Lee, *Phys. Rev. B* **46**, 8434 (1992).
- [24] K.-Y. Yang, T. M. Rice, and F.-C. Zhang, *Phys. Rev. B* **73**, 174501 (2006).
- [25] A. Greco, *Phys. Rev. Lett.* **103**, 217001 (2009).
- [26] E. Cappelluti and R. Zeyher, *Phys. Rev. B* **59**, 6475 (1999).
- [27] M. Bejas, A. Greco, and H. Yamase, *Phys. Rev. B* **86**, 224509 (2012).
- [28] D. J. Scalapino, *Rev. Mod. Phys.* **84**, 1383 (2012).
- [29] E. Demler, S. Sachdev, and Y. Zhang, *Phys. Rev. Lett.* **87**, 067202 (2001).
- [30] E. G. Moon and S. Sachdev, *Phys. Rev. B* **80**, 035117 (2009).
- [31] T. Das, R. S. Markiewicz, and A. Bansil, *Phys. Rev. B* **85**, 064510 (2012).
- [32] C. M. Varma, *Phys. Rev. B* **55**, 14554 (1997).
- [33] H. Yamase and H. Kohno, *J. Phys. Soc. Jpn.* **69**, 2151 (2000).
- [34] S. A. Kivelson, I. P. Bindloss, E. Fradkin, V. Oganesyan, J. M. Tranquada, A. Kapitulnik, and C. Howald, *Rev. Mod. Phys.* **75**, 1201 (2003).
- [35] M. H. Fischer and E.-A. Kim, *Phys. Rev. B* **84**, 144502 (2011).
- [36] M. Hashimoto, R.-H. He, K. Tanaka, J.-P. Testaud, W. Meevasana, R. G. Moore, D. Lu, H. Yao, Y. Yoshida, H. Eisaki, T. P. Devereaux, Z. Hussain, and Z.-X. Shen, *Nat. Phys.* **6**, 414 (2010).
- [37] R.-H. He, M. Hashimoto, H. Karapetyan, J. D. Koralek, J. P. Hinton, J. P. Testaud, V. Nathan, Y. Yoshida, H. Yao, K. Tanaka, W. Meevasana, R. G. Moore, D. H. Lu, S.-K. Mo, M. Ishikado, H. Eisaki, Z. Hussain, T. P. Devereaux, S. A. Kivelson, J. Orenstein, A. Kapitulnik, and Z.-X. Shen, *Science* **331**, 1579 (2011).
- [38] O. J. Lipscombe, B. Vignolle, T. G. Perring, C. D. Frost, and S. M. Hayden, *Phys. Rev. Lett.* **102**, 167002 (2009).
- [39] P. A. Lee, *Phys. Rev. X* **4**, 031017 (2014).
- [40] E. Berg, E. Fradkin, S. A. Kivelson, and J. M. Tranquada, *New J. Phys.* **11**, 115004 (2009).
- [41] I. M. Vishik, M. Hashimoto, R.-H. He, W.-S. Lee, F. Schmitt, D. Lu, R. G. Moore, C. Zhang, W. Meevasana, T. Sasagawa, S. Uchida, K. Fujita, S. Ishida, M. Ishikado, Y. Yoshida, H. Eisaki, Z. Hussain, T. P. Devereaux, and Z.-X. Shen, *Proc. Natl. Acad. Sci. USA* **109**, 18332 (2012).
- [42] M. Hashimoto, E. A. Nowadnick, R.-H. He, I. M. Vishik, B. Moritz, Y. He, K. Tanaka, R. G. Moore, D. Lu, Y. Yoshida, M. Ishikado, T. Sasagawa, K. Fujita, S. Ishida, S. Uchida, H. Eisaki, Z. Hussain, T. P. Devereaux, and Z.-X. Shen, *Nat. Mater.* **14**, 37 (2015).
- [43] S. Nandi, M. G. Kim, A. Kreyssig, R. M. Fernandes, D. K. Pratt, A. Thaler, N. Ni, S. L. Bud'ko, P. C. Canfield, J. Schmalian, R. J. McQueeney, and A. I. Goldman, *Phys. Rev. Lett.* **104**, 057006 (2010).
- [44] N. Ni, M. E. Tillman, J.-Q. Yan, A. Kracher, S. T. Hannahs, S. L. Bud'ko, and P. C. Canfield, *Phys. Rev. B* **78**, 214515 (2008).
- [45] R. M. Fernandes, D. K. Pratt, W. Tian, J. Zarestky, A. Kreyssig, S. Nandi, M. G. Kim, A. Thaler, N. Ni, P. C. Canfield, R. J. McQueeney, J. Schmalian, and A. I. Goldman, *Phys. Rev. B* **81**, 140501 (2010).
- [46] J.-B. Wu, M.-X. Pei, and Q.-H. Wang, *Phys. Rev. B* **71**, 172507 (2005).
- [47] T. Kondo, Y. Hamaya, A. D. Palczewski, T. Takeuchi, J. S. Wen, Z. J. Xu, G. Gu, J. Schmalian, and A. Kaminski, *Nat. Phys.* **7**, 21 (2011).
- [48] T. Kondo, T. Takeuchi, A. Kaminski, S. Tsuda, and S. Shin, *Phys. Rev. Lett.* **98**, 267004 (2007).
- [49] K. Terashima, H. Matsui, T. Sato, T. Takahashi, M. Kofu, and K. Hirota, *Phys. Rev. Lett.* **99**, 017003 (2007).
- [50] A. Kaminski, T. Kondo, T. Takeuchi, and G. Gu, *Philos. Mag.* **95**, 453 (2015).
- [51] T. P. Devereaux and R. Hackl, *Rev. Mod. Phys.* **79**, 175 (2007).
- [52] B. Loret, S. Sakai, Y. Gallais, M. Cazayous, M.-A. Méasson, A. Forget, D. Colson, M. Civelli, and A. Sacuto, *Phys. Rev. Lett.* **116**, 197001 (2016).
- [53] W. Guyard, A. Sacuto, M. Cazayous, Y. Gallais, M. Le Tacon, D. Colson, and A. Forget, *Phys. Rev. Lett.* **101**, 097003 (2008).

- [54] W. Guyard, M. Le Tacon, M. Cazayous, A. Sacuto, A. Georges, D. Colson, and A. Forget, *Phys. Rev. B* **77**, 024524 (2008).
- [55] S. Blanc, Y. Gallais, M. Cazayous, M. A. Méasson, A. Sacuto, A. Georges, J. S. Wen, Z. J. Xu, G. D. Gu, and D. Colson, *Phys. Rev. B* **82**, 144516 (2010).
- [56] M. Le Tacon, A. Sacuto, A. Georges, G. Kotliar, Y. Gallais, D. Colson, and A. Forget, *Nat. Phys.* **2**, 537 (2006).
- [57] A. Sacuto, Y. Gallais, M. Cazayous, S. Blanc, M.-A. Méasson, J. Wen, Z. Xu, G. Gu, and D. Colson, *C. R. Phys.* **12**, 480 (2011).
- [58] A. Kanigel, M. R. Norman, M. Randeria, U. Chatterjee, S. Souma, A. Kaminski, H. M. Fretwell, S. Rosenkranz, M. Shi, T. Sato, T. Takahashi, Z. Z. Li, H. Raffy, K. Kadowaki, D. Hinks, L. Ozyuzer, and J. C. Campuzano, *Nat. Phys.* **2**, 447 (2006).
- [59] L. Chauvière, Y. Gallais, M. Cazayous, M. A. Méasson, A. Sacuto, D. Colson, and A. Forget, *Phys. Rev. B* **82**, 180521 (2010).
- [60] S. Chakravarty, H.-Y. Kee, and K. Volker, *Nature (London)* **428**, 53 (2004).
- [61] R. B. Laughlin, *Phys. Rev. Lett.* **112**, 017004 (2014).
- [62] R. B. Laughlin, *Phys. Rev. B* **89**, 035134 (2014).
- [63] W.-G. Yin and W. Ku, *Phys. Rev. B* **79**, 214512 (2009).
- [64] M. Ogata and A. Himeda, *J. Phys. Soc. Jpn.* **72**, 374 (2003).
- [65] W.-S. Wang, X.-M. He, D. Wang, Q.-H. Wang, Z. D. Wang, and F. C. Zhang, *Phys. Rev. B* **82**, 125105 (2010).
- [66] T. Das, R. S. Markiewicz, and A. Bansil, *Phys. Rev. B* **77**, 134516 (2008).
- [67] J. D. Sau and S. Sachdev, *Phys. Rev. B* **89**, 075129 (2014).
- [68] A. M. Gabovich and A. I. Voitenko, *Physica C: Superconductivity* **503**, 7 (2014).
- [69] Kordyuk, *Low Temp. Phys.* **41**, 319 (2015).
- [70] Y. Yildirim and W. Ku, *Phys. Rev. X* **1**, 011011 (2011).
- [71] Y. Wang, Z. A. Xu, T. Kakeshita, S. Uchida, S. Ono, Y. Ando, and N. P. Ong, *Phys. Rev. B* **64**, 224519 (2001).
- [72] L. Li, Y. Wang, S. Komiyama, S. Ono, Y. Ando, G. D. Gu, and N. P. Ong, *Phys. Rev. B* **81**, 054510 (2010).
- [73] J. L. Tallon, J. G. Storey, and J. W. Loram, *Phys. Rev. B* **83**, 092502 (2011).
- [74] H.-Y. Lu and Q.-H. Wang, *Phys. Rev. B* **75**, 094502 (2007).
- [75] V. J. Emery and S. A. Kivelson, *Physica C* **263**, 44 (1996).
- [76] C. M. Varma, S. Schmitt-Rink, and E. Abrahams, *Solid State Commun.* **62**, 681 (1987).
- [77] M. J. Lawler, K. Fujita, J. Lee, A. R. Schmidt, Y. Kohsaka, C. K. Kim, H. Eisaki, S. Uchida, J. C. Davis, J. P. Sethna, and E.-A. Kim, *Nature (London)* **466**, 347 (2010).
- [78] W. Li, W.-G. Yin, L. Wang, K. He, X. Ma, Q.-K. Xue, and X. Chen, *Phys. Rev. B* **93**, 041101(R) (2016).
- [79] D. Volja, W.-G. Yin, and W. Ku, *Europhys. Lett.* **89**, 27008 (2010).
- [80] Y. M. Dai, B. Xu, B. Shen, H. H. Wen, J. P. Hu, X. G. Qiu, and R. P. S. M. Lobo, *Phys. Rev. B* **86**, 100501(R) (2012).
- [81] K. M. Taddei, J. M. Allred, D. E. Bugaris, S. Lapidus, M. J. Krogstad, R. Stadel, H. Claus, D. Y. Chung, M. G. Kanatzidis, S. Rosenkranz, R. Osborn, and O. Chmaissem, *Phys. Rev. B* **93**, 134510 (2016).
- [82] J. Allred, K. Taddei, D. Bugaris, M. Krogstad, S. Lapidus, D. Chung, H. Claus, M. Kanatzidis, D. Brown, J. Kang *et al.*, *Nat. Phys.* **12**, 493 (2016).
- [83] A. Böhmer, F. Hardy, L. Wang, T. Wolf, P. Schweiss, and C. Meingast, *Nat. Commun.* **6**, 7911 (2015).
- [84] S. Avcı, O. Chmaissem, J. Allred, S. Rosenkranz, I. Eremin, A. V. Chubukov, D. Bugaris, D. Chung, M. Kanatzidis, J.-P. Castellan *et al.*, *Nat. Commun.* **5**, 3845 (2014).
- [85] J. Brinckmann and P. A. Lee, *Phys. Rev. Lett.* **82**, 2915 (1999).
- [86] Q. Yuan, X.-Z. Yan, and C. S. Ting, *Phys. Rev. B* **74**, 214503 (2006).
- [87] K.-Y. Yang, W. Q. Chen, T. M. Rice, M. Sgrist, and F.-C. Zhang, *New J. Phys.* **11**, 055053 (2009).